The function of plasma membrane V-ATPases in breast cancer growth and metastasis

A thesis submitted by

Mohammed Abdullah Alshagawi

In partial fulfillment of the requirements for the degree of

Master of Science

In

Pharmacology and Drug Development

Tufts University

Graduate School of Biomedical Sciences

August 2022

Advisor: Michael Forgac, PhD

Co-Advisor: James Baleja, PhD

Abstract

The Vacuolar ATPase is an ATP-driven proton pump which functions mainly to maintain cell homeostasis through controlling intracellular pH. The V-ATPase is present at the plasma membrane of specialized cell types, including osteoclasts and renal intercalated cells, as well as several cancer cell types. It is hypothesized that the V-ATPases are a major contributor to the survival, growth, and metastasis of tumor cells. They are thought to contribute to cell survival through removal and secretion of excess acid from the cytosol to the extracellular space to maintain a neutral intracellular pH. V-ATPases may also contribute to cell invasion through acidification of the extracellular space, which will create an acidic environment for secreted proteases like cathepsins, which can, in turn, degrade the extracellular matrix and allow invasion of new tissues.

The targeting of V-ATPase to the plasma membrane is controlled by isoforms of subunit a, and we have previously shown that isoforms a3 and a4, which target V—ATPases to the surface of osteoclasts and renal intercalated cells, respectively, are important for the migration and invasion of several breast cancer cell lines *in vitro*. Using CRISPR-mediated gene disruption to selectively knock out each of the four isoforms of subunit a, our lab has shown that a4 is important for V-ATPase localization to the plasma membrane and in vitro invasion and migration of 4T1-12B mouse breast cancer cells. Here, we report that a4 is also critical for tumor growth and metastasis in vivo following implantation of 4T1-12B in mouse mammary fat pads. BALB/c mice bearing $a4^{-/-}$ 4T1-12B allografts had dramatically reduced tumor growth and a significant decrease in organ metastasis as assessed using bioluminescence ex vivo imaging.

Additionally, our lab has shown previously that a synthetic, inhibitory, bivalent nanobody targeting an extracellular epitope on subunit c can reduce invasion and migration of 4T1-12B cells in vitro. Here, we report that this nanobody treatment significantly reduces metastasis to lung of 4T1-12B cells. Our results suggest that plasma membrane V-ATPases are a novel therapeutic target to decrease breast cancer growth and metastasis.

Acknowledgments

First and foremost, I am extremely grateful to my advisor, Michael Forgac, for his invaluable guidance that carried me through all the stages of this work, from experimental design and analyzing results to thesis writing. Thank you, Mike, for supporting my ideas, trusting my abilities, and training me on how to think critically as a student of science. It was my pleasure working with and learning from you.

I want to give my deepest appreciation to previous and current members of the Forgac lab: Kevin Su and Zhen Li. Thank you, Kevin, for welcoming me into the lab during the winter of 2021, learning laboratory techniques was a bit challenging, but you made it easier. And Zhen, without your efforts, my animal experiments would have undoubtedly been more difficult, I wish you all the best in your future endeavors.

I would also like to thank my Co-Mentor, James Baleja, for helping me with my thesis writing. And to Dr. Amy Yee, Dr. Eric Paulson, and everyone in the Yee lab, thank you for having me as a rotation student.

To my friend, Ahmed, thank you for the endless support.

And lastly, to my family overseas, my gratitude for you can hardly be expressed in words. I could have never made it without you.

Table of contents

List of Tables

List of Figures

List of Copyrighted Materials Used

Forgac, M. (2007). *Vacuolar ATPases: Rotary proton pumps in physiology and pathophysiology.* Nature Reviews Molecular Cell Biology, 8(11), 917–929.

Su, Kevin L, (2021). *The role of plasma membrane V-ATPases in breast cancer metastasis.* ProQuest Dissertations Publishing.

List of Abbreviations

a1–a4, V-ATPase subunit a, isoforms a1 through a4
ADP, adenosine diphosphate
ATP, adenosine triphosphate
ConA, concanamycin A
CRISPR, Clustered regularly interspaced short palindromic repeats
DMEM, Dulbecco's modified Eagle medium
DMSO, dimethyl sulfoxide
FBS, fetal bovine serum
GABA, Gamma-aminobutyric acid
IVIS, in vivo imaging system
Kda, kilodalton
KO, Knockout
PBS, Phosphate buffered saline
Pen/strep, penicillin/streptomycin
RNA, ribonucleic acid
V-ATPase, vacuolar H+-ATPase
V0, V-ATPase membrane domain
V1, V-ATPase peripheral domain

Chapter 1: Introduction

1.1 V-ATPase Structure and Mechanism

The Vacuolar ATPase is a large multi-subunit complex that functions in a variety of compartments in the cell as an ATP-driven proton pump (1, 2). The complex consists of two domains that operate by a rotary mechanism (1). V_1 which is a 650 kDa cytosolic domain that performs ATP hydrolysis, and V_0, which is 260 kDa, is a membrane-embedded domain that allows proton translocation from the cytoplasm to the extracellular space or to the lumen of intracellular compartments (1, 2).

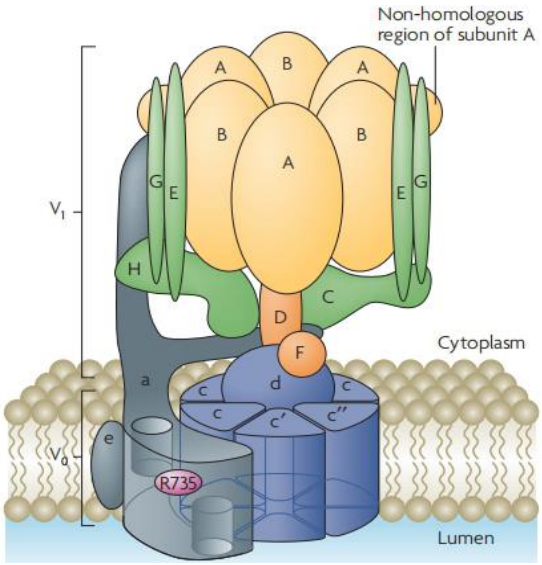

Figure 1.1 *The structure of the vacuolar ATPase.* The V-ATPase is a multi-subunit complex composed of a peripheral V1 domain that performs ATP hydrolysis, and V0, a membrane-embedded domain, that allows proton translocation. Reprinted with permission from Forgac, Michael (2007). Vacuolar ATPases: Rotary proton pumps in physiology and pathophysiology. *Nature Reviews Molecular Cell Biology, 8(11), 917–929.*

V1 is composed of eight different subunits (A, B, C, D, E, F, G, H) in a stoichiometry of A3B3CDE3FG3H, whereas V0 is composed of six different subunits (a,

d, e, c, c′, and c″) in a stoichiometry of ac9c″de (yeast have a c′ subunit that replace one of the c subunits) (2).

The V-ATPase has a similar structure and mechanism to the F-type ATP-Synthase (F-ATPase), as both are large, multisubunit complexes that operate by a rotary mechanism, but instead of synthesizing ATP from ADP using the proton motive force, the V-ATPase always performs active proton transport (1, 3). The A3B3 catalytic hexameric head in the V1 domain is connected to the central and peripheral stalks (1). The central stalk is composed of subunits D, F, and d connected to the proteolipid ring of c subunits, and together they function as a rotor (1). ATP hydrolysis, which occurs at the interfaces of the A and B subunits, initiates the rotation of the central stalk, hence driving the rotation of the proteolipid ring (1). Reversible protonation and deprotonation of a glutamic acid residue on each proteolipid subunit occurs during proton transport. During rotation, each protonated glutamic acid will interface with the luminal hemichannel in subunit a. resulting in the stabilization of deprotonation of the glutamic acid by an arginine residue in subunit a, thus releasing of the proton into the lumen.(1, 2).

1.2 The function of the V-ATPase

1.2.1 Intracellular V-ATPases

The V-ATPase is active in multiple compartments in the cell and is mainly responsible for controlling luminal pH, which is crucial for normal physiology and homeostasis in the cell (1, 4). In sorting endosomes, the V-ATPase will lower the pH to allow ligand-receptor complexes to be uncoupled following receptor-mediated endocytosis (1). This allows the unoccupied receptor to return to the cell membrane. The

rate of uptake of ligands, such as low-density lipoprotein and transferrin, is heavily dependent on receptor recycling (5). Rates of recycling are also an important factor in the control of receptor density which controls the sensitivity to hormones such as insulin and growth factors such as epidermal growth factor.

Certain pathogens, such as influenza and Ebola viruses, can use the low pH inside the endosome to enter the cell and reach the cytoplasm. Viral RNA can be delivered to the cytosol by fusion of viruses with the endosomal membrane, which is facilitated by the acidic environment (6). Several toxins, such as diphtheria and anthrax, can also use the endosomal acidic pH to gain entry to the cytoplasm (1, 7). The V-ATPase also has a role in the storage of neurotransmitters, such as glutamate, by creating the positive interior membrane potential in synaptic vesicles (1). Other neurotransmitters, such as GABA and noradrenaline, use proton antiporters to be stored in synaptic vesicles (1, 8).

Autophagy is an essential process for the degradation of intracellular macromolecules (9). V-ATPases expressed on the lysosome facilitate autophagy (10). In this process, macromolecules are engulfed within double-membrane vesicles, called autophagosomes, which will subsequently fuse with the lysosome to form autolysosomes. Autolysosomes are responsible for the degradation of luminal contents. Catabolites eventually will return to the cytosol for recycling (11). Acidification of the lysosome by the V-ATPase is essential for this process (12, 13). Selective inhibition of the V-ATPases using Bafilomycin A1, which enters the cell and inhibits intracellular V-ATPases, will prevent the fusion of the autophagosome with lysosomes, thus inhibiting autophagy (14).

1.2.2 Plasma membrane V-ATPase

Not all cell types express the V-ATPase on the plasma membrane. In fact, the V-ATPase is targeted to the plasma membrane of only a few specialized mammalian cells (1). Targeting of V-ATPases is controlled by isoforms of subunit a. In mammals, there are four genes that encode subunit a (a1-a4) (15), a1 and a2 are primarily intracellular, with a1 targeted to synaptic vesicles and presynaptic plasma membranes (16) whereas the a2 isoform is targeted to apical endosomes in renal proximal tubule cells (17). a3 is found in the plasma membrane of osteoclasts (18), where V-ATPases promote acidification of the space between the osteoclast and bone to facilitate bone resorption. A severe form of osteopetrosis occurs in humans which have mutations in the a3 isoform of subunit a (1). The V-ATPase is also present in the plasma membrane of renal alpha intercalated cells, where a4 subunit is responsible for targeting to the plasma membrane (1). Intercalated cells sense and adjust plasma pH using V-ATPases expressed in the apical membrane, where they pump excess acid into the urine. Mutations in the a4 isoform of subunit a cause renal tubular acidosis in humans (19, 20). Similarly, the V-ATPases at the apical membrane of clear cells of the epididymis are crucial for sperm growth and storage (1), (21). Mutations in the epididymal V-ATPase cause infertility in mice (22).

1.3 V-ATPase in cancer

Evidence from our lab and others has suggested that V-ATPases are a major contributor to the survival, growth and metastasis of tumor cells (23). Plasma membrane V-ATPases can remove excess acid in the cytosol and secret it to the extracellular space to maintain a neutral pH inside the cell (24). The low pH in the cytosol is caused mainly

by a hypoxic microenvironment and the consequent reliance by tumor cells on glycolytic metabolism that produces metabolic acids (25).

By blocking the pump and inhibiting acid secretion, V-ATPase inhibitors such as Bafilomycin induce apoptosis in cancer cells (26, 27). Localization of the V-ATPase to the plasma membrane has been observed in a number of human breast and lung samples and different cancer cell lines (28, 29, 30, 31, 32, 33). Another mechanism by which the V-ATPase may promote tumor survival is by compromising the effectiveness of chemotherapeutic agents since several cancer drugs are weak bases and the acidic microenvironment within lysosomes will sequester drug molecules within the lumen and prevent them from reaching their cellular targets (4, 34, 35). This may explain the synergistic effect of V-ATPase inhibitors with some chemotherapeutic agents (36, 37). Patients who die from cancer die primarily due to metastasis. Metastasis is a multi-step process characterized by the dissociation of tumor cells from the primary site and invasion of the cells into the bloodstream or the lymphatic system, followed by migration to a secondary site or organ (38). Because the V-ATPase acidifies the extracellular environment surrounding invasive cancer cells, it will create an acidic microenvironment that activates secreted proteases like cathepsins, which require a low pH for activity. These proteases degrade the extracellular matrix and allow tumor cells to invade new tissues (39, 40). Thus, V-ATPases have been shown to promote invasiveness, one of the essential properties of tumor cells (1, 4, 40).

The V-ATPase is highly localized to the plasma membrane in highly invasive MCF10CA1a cells compared to non-invasive MCF10a cells (30). The targeting of the pump to the plasma membrane is controlled by isoforms of subunit a. It was reported that

the a3 isoform is upregulated in invasive MDA-MB 231 and MCF10CA1a cells compared to non-invasive MCF7 and MCF10a cells (30, 31). Knockdown of a3 using isoform-specific small interference RNA significantly reduces in vitro invasion and migration of MDA-MB-231 and MCF10CA1a cells (30, 31). Importantly, overexpression of the a3 isoform increases the plasma membrane localization of V-ATPases as well as invasion by non-invasive MCF10a cells (30). As mentioned above, bafilomycin and concanamycin can inhibit the invasion and migration of several cancer cell lines (30), (31, 28, 29, 33, 32). Because bafilomycin and concanamycin are membrane-permeant inhibitors of the V-ATPase, they will inhibit intracellular V-ATPases as well as cell surface V-ATPases, limiting their use clinically due to system toxicity. It is therefore important to test whether selective inhibition of plasma membrane V-ATPases will reduce invasion as effectively as membrane permeant V-ATPase inhibitors. MDA-MB-231 cells were transfected with a v5 epitope-tagged version of subunit c in which the epitope tag was exposed on the cell surface (40). Our lab showed that by using an anti-v5 antibody, activity of the V-ATPase at the plasma membrane was inhibited (40).

Moreover, this antibody inhibited invasion of MB231 cells, indicating that it is plasma membrane V-ATPases that are essential for tumor cell invasiveness (40). Similar results were obtained using a membrane impermeant V-ATPase inhibitor, bafilomycin-biotin which was bound to streptavidin (40). Consistent with the essential role of cell surface V-ATPases in cancer cell invasion, the a3 isoform was upregulated at the RNA level in 43 of 43 human breast tissue samples relative to normal breast tissue, especially in samples from stage 3 and 4 patients (28). In addition, the highest level of expression of a3 at the protein level was observed in invasive breast carcinoma relative to solid tumors

and normal tissue, as assessed by immunohistochemistry of human breast tissue samples (28). Recently, CRISPR-mediated gene disruption of isoforms of subunit a in the highly metastatic mouse 4T1-12B breast cancer cell line has shown that the a4 isoform is critical for in vitro invasion and migration of these cells (33). Overall, these studies support the hypothesis that plasma membrane V-ATPases represent an important and novel target to block breast cancer metastasis.

1.4 Thesis Objectives

This thesis aims to further study the function of plasma membrane V-ATPases in breast cancer growth and metastasis in vivo. Chapters 3.1 and 3.2 discuss the role of different a subunit isoforms in promoting tumor growth and metastasis by 4T1-12B cells when implanted orthotopically into BALB/c mice. Chapters 3.3 to 3.5 describe the effect of an inhibitory, bivalent nanobody targeting the c subunit of the V-ATPase on breast cancer cell invasion and migration, as well as the effect of this nanobody on breast tumor growth and metastasis in vivo using the 4T1-12B model system in mice.

Chapter 4 discusses ongoing steps to improve our mouse models and future directions to further explore the role of V-ATPases in breast cancer metastasis.

Chapter 2: Materials and Methods

2.1 Cell culture

CRISPR- mediated knock-out cells were established in the Forgac lab previously (33). 4T1-12B cells were a gift from Dr. Gary Sahagian's lab at Tufts University. Cells were grown in 10 cm tissue culture plates (Thermo Scientific #130182), containing DMEM with phenol red, 25 mM D-glucose, 4 mM 1-glutamine, and 1mM sodium pyruvate (Gibco #11995) supplemented with 10% FBS (Sigma-Aldrich #12306C) and 1% Pen/strep (Gibco #15140). Cells were cultured at 37 C and 5% CO2 in a humidified incubator. Cells were not passaged more than 10 times.

2.2 Transwell invasion and migration assays

In vitro invasion and migration assays were performed as described previously. Briefly, Fluroblock inserts (Falcon #351152), with 8-um pore size were placed into 24 well plates containing 500 ul DMEM supplemented with 10% FBS per well.
For the invasion assay, a final concentration of 20 ug/ul of Matrigel diluted in 1x PBS was used to coat each membrane. Matrigel was left to dry at room temperature overnight under a vacuum.

Then, Matrigel-coated plates were allowed to rehydrate with 200µl of DMEM (no additives) for 2 hours at room temperature. Cells were trypsinized and then diluted to a final concentration of 1.25 x 10^5 cells/ml in DMEM. 1nM concanamycin A or DMSO was added to diluted cells as indicated. For cells treated with nanobody, the selected volume was diluted in PBS. Each condition was done in triplicate.

Cells then were left in the incubator at 37 C and 5% CO2 for an average of 18 hours for invasion and 21 hours for migration. Inserts then were placed into wells containing 4μg/ml Calcein-AM in PBS and incubated for 5 minutes at 37°C in 5% CO2. Wells with migrated cells on the trans side of the membrane were imaged using a Zeiss Axiovert 10 fluorescence microscope.

2.3 Animal Care

Female BALB/c mice aged 6 weeks were purchased from the Jackson Laboratory (Bar Harbor, ME), and housed at the Tufts University animal facility. All in vivo work was approved by and carried out in accordance with the Tufts University Institutional Animal Care and Use Committee. All experiments and procedures were performed at the animal facility at Tufts University.

2.4 in vivo metastasis model

CRISPR-modified 4T1-12B cells were seeded at 1×10^5 cells/cm^2 (approximately 40% confluency) and allowed to attach overnight. When cells were 80% confluent, cells were detached by trypsinization (Gibco #25300054) and verified to be ≥95% viable by trypan blue. Then, cells were centrifuged at 300×*g* for 5 minutes, and the cell pellets were resuspended in DMEM at 1×10^7 cells/ml. 1×10^6 cells/100μl were injected into the intact no. 4 inguinal fat pad of 6-week old female BALB/c mice using a 26-gauge needle. Primary tumor volume was measured weekly for experiment 1 of the KO experiment and three times a week for the remaining trials by caliper measurement, and tumor volume was calculated using the modified ellipsoid formula $(L \times W^2)/2$ (41).

2.5 Bioluminescence imaging

In vivo and ex vivo imaging was performed on the first-day post-implantation for the KO experiments and the first nanobody experiment to confirm the correct implantation of cells. A fresh luciferin solution was prepared before imaging by dissolving XenoLight D-luciferin monopotassium salt (Perkin Elmer #122799) in PBS (10mg/ml). The luciferin solution was filter-sterilized, and 100µl was injected into each mouse intraperitoneally. Mice were anesthetized with a 2.5%/97.5% isoflurane/O_2 mixture using a Caliper Life Sciences XGI-8 Gas Anesthesia System and imaged 10 minutes post-luciferin injection using a Perkin Elmer IVIS SpectrumCT In Vivo Imaging System. At study endpoint (or when humane endpoints were reached), animals were sacrificed, and organs were removed and imaged *ex vivo* following the same luciferin injection protocol. Because the intensity of the signal from the primary tumor prevented detection of metastases in the intact mice in the first KO trial, live animal imaging was not performed after the initial KO experiment.

2.6 Statistical analysis

P values were calculated using an unpaired student T-test

Chapter 3: Results

3.1 CRISPR-mediated disruption of the a4 isoform in 4T1-12B cells reduces tumor growth in vivo

Our lab has previously established selected clonal 4T1-12B cell lines in which each line lacks one of the four isoforms that encode subunit a by implementing CRISPR-mediated gene disruption (33). The level of expression of subunit a in each clone was characterized using western blot analysis (33). First, we proceeded with *in vivo* tumor cell implantation. 4T1-12B cells were orthotopically implanted by injecting $1x10^6$ cells in 100 ul DMEM into the intact no. 4 inguinal fat pad of 6-week-old, female BALB/c mice. ten mice per group were used in each of two independent trials. Tumor volume over time was monitored until humane endpoint criteria were met, or at the study endpoint (6 weeks), as described in chapter 2.4. The tumor measurement started on day 7 when most primary tumors were palpable. The primary tumor volumes were determined by external caliper measurement weekly for experiment 1 and every three days for experiment 2. The mean tumor volume for all 50 mice was 91 ± 14 mm^3, with no statistically significant differences between the different a isoform knockout groups at day 10. In the next measurement, all mice had palpable tumors except for 1 mouse in the $a4^{-/-}$ group, which remained tumor-free until the end of the trial. By comparison, on day 10 of the second trial, 49 of 49 mice presented with palpable tumors at the mammary fat pad. 10 mice per group were assigned to each group, except for the a3 group, where only 9 mice were injected because of the lack of enough cells at day 0. Figure 3.1A shows the primary tumor growth curves. Asterisks indicate statistically significant mean tumor volumes different from the negative control group on a given day (* $p < 0.05$). For Experiment 1, the a4-/- group had reduced tumor volume compared to the control group starting at day 27, whereas the a2 -/- group had

larger tumors than controls starting at day 20. Results were similar for Experiment 2, the a4$^{-/-}$ group had smaller tumors than the control group starting at day 17 while the a2$^{-/-}$

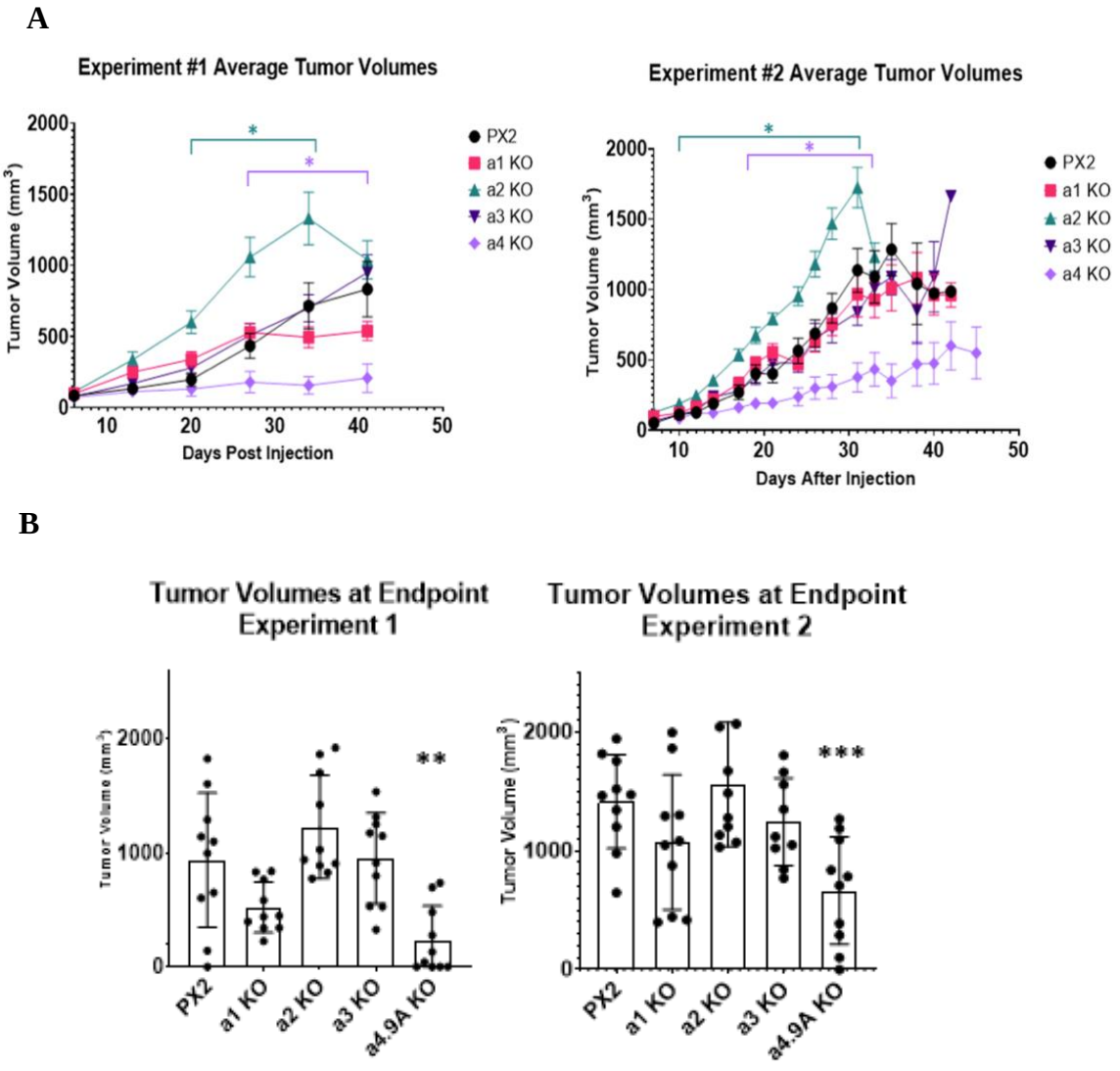

Figure 3.1 *Tumor volumes of primary tumors in BALB/c mice bearing negative control and a isoform knockout 4T1-12B allografts.* Negative control and CRISPR-mediated a isoform knockout 4T1-12B cells were implanted into the mammary fat pads of female BALB/c mice, as described in chapter 2.4. Primary tumor volumes were determined by caliper measurements taken weekly for Experiment 1 and 3 times a week for Experiment 2. Values represent the mean. (* $p < 0.05$, error bars represent SEM.) B) Tumor volumes for all mice measured at time of takedown. (** $p < 0.005$, *** $p < 0.0005$, error bars represent SEM.) (For Experiment 1, n=10 for PX2, n=10 for a1 KO, n=10 for a2 KO, n=10 for a3 KO, n=10 for a4 KO. For Experiment 2, n=10 for PX2, n=10 for a1 KO, n=10 for a2 KO, n=9 for a3 KO, n=10 for a4 KO.

group had significantly larger tumors than negative controls starting at Day 14 (Figure 3.1A). Tumor volumes for each mouse were compared at the study endpoint. For Experiment 1, the mean tumor volume was 1221 ± 104 mm^3 in the control group and 439 ± 93 mm^3 in the $a4^{-/-}$ group, showing a significant reduction in tumor growth (Figure 3.1B). Note that throughout the 6-weeks duration of each study, several mice were euthanized due to low body condition scores or reaching tumor volume endpoint (1500mm^3). Table 3.1 shows the time course of euthanasia of individual mice.

Experiment 1:					
Group	week 1	week 2	week 3	week 4	week 5
PX2	1 mouse	0	0	0	0
a1-/-	0	0	0	0	0
a2-/-	0	0	0	4*	2
a3-/-	0	0	0	0	0
a4-/-	0	0	0	0	1
Experiment 2:					
Group	week 1	week 2	week 3	week 4	week 5
PX2	0	0	0	3	5
a1-/-	0	0	2	1	1
a2-/-	0	0	1	5	4
a3-/-	0	0	0	0	8
a4-/-	0	0	0	0	2

Table 3.1 *Time course of euthanasia of individual mice*. Numbers in the table represent the number of mice that had to be euthanized because of reaching humane endpoint criteria unless noted otherwise **(* =** three euthanized and one found dead).

3.2 CRISPR-mediated disruption of the a4 isoform in 4T1-12B cells reduces tumor metastasis in vivo

One of the main advantages of using the 4T1-12B breast cancer model is the metastatic properties of cells in immunocompetent mice. Thus, in addition to recording the growth of the primary tumors, metastasis was measured at the end of the study by euthanizing mice and collecting the brain, heart, kidneys, liver, lungs, spleen, and hind legs for *ex vivo* imaging.

Cell Line	Spleen	Liver	Kidney/ Adrenals	Lungs	Heart	Brain	Limbs
PX2	3(15)	3(15)	2(15)	15(15)	0(15)	1(15)	15(15)
a1 KO	0(8)	1(8)	0(8)	3(8)	0(8)	0(8)	8(8)
a2 KO	1(10)	2(10)	1(10)	10(10)	0(10)	0(10)	10(10)
a3 KO	0(9)	0(9)	0(9)	9(9)	0(9)	0(9)	9(9)
a4.5A	0(10)	0(10)	0(10)	0(10)	0(10)	0(10)	10(10)
a4.9A	0(9)	0(9)	0(9)	1(9)	0(9)	0(9)	9(9)

Table 3.2 *Comparison of frequency of metastases to various organs in BALB/C mice bearing negative control and CRISPR mediated a isoform knockout 4T1-12B allografts.* Table shows the frequency of metastasis seen in organs imaged ex vivo using IVIS bioluminescence.

Because the signal from the primary tumors in experiment 1 interfered with the luminescence signal of other organs, metastasis was not measurable in vivo. For experiment 2, organs were imaged separately to avoid signal interference from the primary tumor. Metastasis data are shown in Table 3.2. As shown, all mice implanted with the PX2 control cells had metastases in lungs and bone (limbs). On the other hand, the initial a4 knockout clone (a 4.9A) showed 0 metastases to any organ other than bone. For the a 4.5A knockout group, only one out of nine mice developed metastasis to the lung. All other organs had no metastasis except for bone. The a2 knockout group developed metastases

with relatively similar frequency as the control group. In addition, knockout of a1 also significantly reduced metastasis to the lung (three out of eight mice).

To further assess the effect of a isoform knockout on tumor metastasis, the luminescence intensity in bones was quantified and compared.

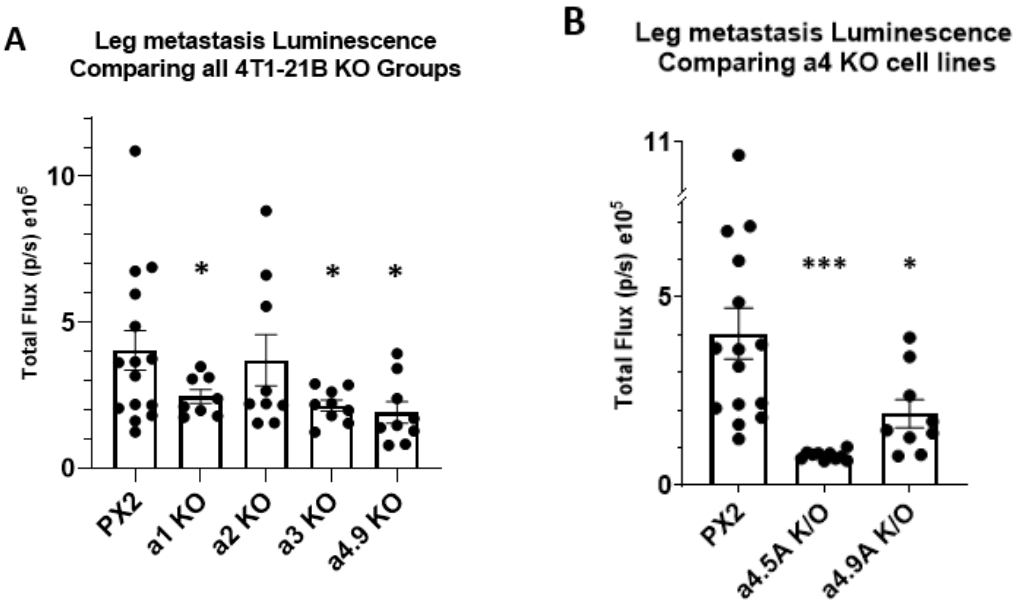

Figure 3.2 *Luminescence intensity of bone metastases in BALB/c mice bearing negative control and CRISPR mediated a isoform knockout 4T1-12B allografts*. Mice were injected with luciferin as described in Chapter 2.5. At study endpoint, or after reaching humane endpoint criteria, then, mice were sacrificed, and hind limbs were imaged ex vivo. A) Luminescence measured in hind limbs comparing KO clones of each subunit a isoform. (* $p < 0.05$, error bars represent SEM.) B) Luminescence measured in hind limbs comparing control to two different a4 KO clones. (* $p < 0.05$, *** $p < 0.0005$, error bars represent SEM.) (n=15 for PX2, n=8 for a1 KO, n=10 for a2 KO, n=9 for a3 KO, n=10 for a4/a4.9A KO, n=9 for a4.5A KO).

As shown in Figure 3.2A, knockout of all isoforms except a2 reduced the luminescence intensity of bone metastases compared to control cells. Furthermore, as

shown in Figure 3.2B, luminescence intensity of bone metastases derived from the a 4.5A knockout clone were further reduced relative to the a 4.9A knockout clone. These results suggest that, although all groups, including the a4 group, had detectable bone metastasis, there is a reduced number of tumor cells in bone with knockout of a4 compared to the control group. The a1 and a3 groups also had reduced bone luminescence but the difference was less than seen in the a4 group.

3.3 A synthetic nanobody targeting subunit c inhibits in vitro invasion and migration

As discussed in chapter 1.3, our lab showed inhibition of in vitro invasion and migration of MB231 cells by inhibition of plasma membrane V-ATPases activity using a monoclonal antibody targeting a synthetic V5 epitope tag fused to an extracellular domain of subunit c (40).

We therefore collaborated with a company (Proteogenix), to develop and engineer a synthetic antibody designed with two VHH nanobodies connected by a human CH1 and hinge region. The peptide used to screen for nanobody binders corresponded to the C-terminus of subunit c, which is exposed on the outside of the cell. This engineered antibody will have a similar structure to an IgG antibody, but with a lower molecular weight. Transwell invasion and migration assays were performed using 4T1-12B cells as described in Chapter 2.2.

Concanamycin (ConA) was dissolved in DMSO, hence equivalent volume of DMSO was used as its control, Since the nanobody was suspended in PBS, we used equivalent volumes of PBS for each nanobody dilution as a control. 4T1-12B Cells

treated with the nanobody showed a ~53% reduction in cell migration and ~83% reduction in cell invasion (Figure 3.3A, 3.3B).

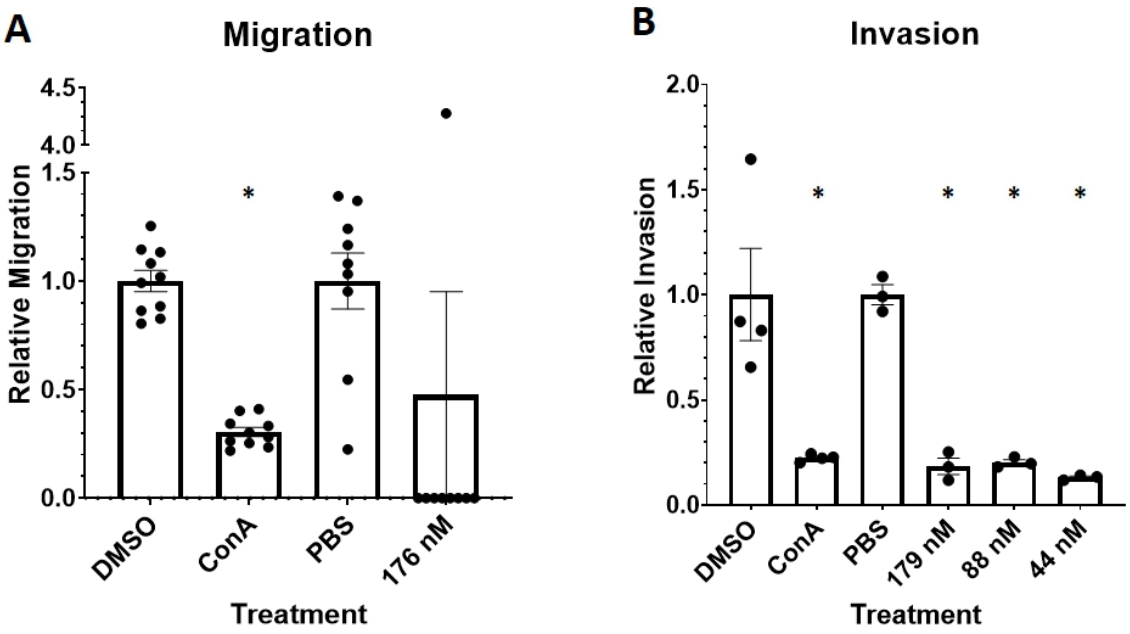

Figure 3.3 *Synthetic nanobody targeting subunit c inhibits transwell migration and invasion*. Transwell migration and invasion assays were performed as described in chapter 2.2. Cells were treated with DMSO, 1 nM ConA, 100 μL PBS, and different dilutions of nanobody suspended in PBS. (* $p < 0.05$ for treatment vs control. Error bars represent SEM) (Each experiment was done in triplicate. n=3 for migration, n=1 for invasion). Reprinted with permission from Su, Kevin L. (2021). *The role of plasma membrane V-ATPases in breast cancer metastasis.* ProQuest Dissertations Publishing.

8 of 9 wells treated with 176 nM nanobody showed no cell migration (Figure 3.3A). invasion was also inhibited at the lowest concentrations (44 nM), which showed approximately 80% inhibition (Figure 3.3B), suggesting that this antibody may be a more potent inhibitor of invasion than migration, this reagent is thus a promising potential therapeutic to inhibit plasma membrane V-ATPases in vivo and to prevent circulating cancer cells from invading tissues and initiating metastasis.

3.4 A low dose of the nanobody against subunit c reduces 4T1-12B metastasis to the lungs in vivo

Our lab has showed that the synthetic nanobody that targets subunit c can significantly decrease invasion and migration in vitro using the 4T1-12B cell line. For our first in vivo trial, we injected 100 ul of 0.32 mg/ml of the nanobody in PBS twice a week for the treatment group and an equivalent volume of PBS for the control group. Primary tumor volumes were determined by using an external caliper (3 measurements per week) until humane endpoint criteria were met or at the study endpoint (6 weeks). Figure 3.4 shows no statistically significant difference between tumor volumes of the two groups at the study endpoints.

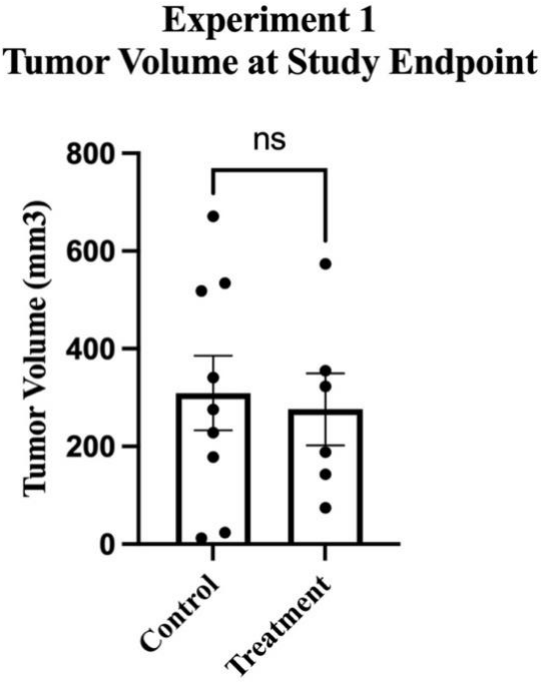

Figure 3.4 *Primary tumor volumes of BALB/c mice treated with or without synthetic nanobody against subunit c* (*first trial*). Mice treated with either 32 ug of a synthetic nanobody against subunit c twice weekly or an equivalent volume of PBS. Tumor volumes for all mice were recorded at the time of euthanasia. (N= 7 for treatment, N=9 for control), (P value = 0.7715. error bars represent the SEM).

It should be noted that mouse number 2 and 6 of the treatment group were found dead on day 26. On day 27 all animals were euthanized following injection of luciferin 10 min prior to sacrifice as described in Chapter 2.5 and organs were collected for ex vivo imaging.

Organs collected were as follows: spleen, liver, kidneys, heart, lungs, brain, and hind limbs. Table 3.3 shows a significant reduction in lung metastasis in the treatment group compared to the control (1/6 compared to 5/9). Figure 3.5 shows luciferin signals in the lungs of selected mice in the control group and the absence of a signal in the treatment group.

Groups	Lung	Heart	Kidneys	Spleen	Liver	Brain	(Limps)
Control	(5)/9	0/9	0/9	0/9	0/9	0/9	9/9
Treatment	(1)/6	0/6	0/6	0/6	0/6	(1)/6	5/6

Table 3.3 *Comparison of frequency of metastases to various organs in BALB/c mice treated with or without synthetic nanobody against subunit c (first trial).* Mice treated with either 32 ug synthetic nanobody against subunit c twice weekly or equivalent volume of PBS. Table shows the frequency of metastasis seen in organs imaged ex vivo using IVIS bioluminescence.

We made a further comparison of the luminescence signal in the bone between the two groups and were surprised to see a significant difference between the groups, namely the treatment group showed higher signal intensity in bone compared to the control group (Figure 3.6). Thus, injection of 64 ug/ week of the synthetic nanobody against subunit c significantly reduced lung metastasis in mice without reducing tumor volume.

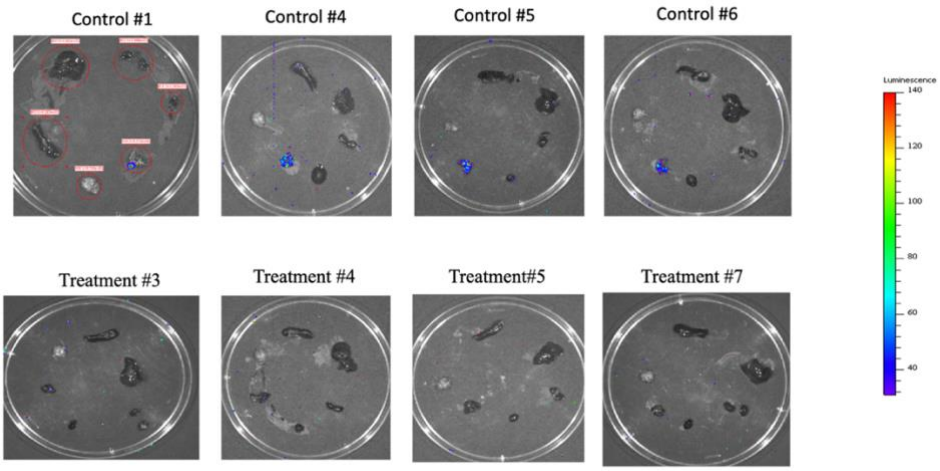

Figure 3.5 *Representative ex vivo organ IVIS images*. Top: Sample images of organs from control group treated with PBS. Organs pictures clockwise from the top are spleen, liver, kidneys, heart, lungs, and brain. Except for Control number 1, organs pictures clockwise from the top are kidneys, heart, lungs, brain, spleen, and liver. Bottom: Sample images of organs from treatment group treated with 64 ug weekly synthetic nanobody against subunit c.

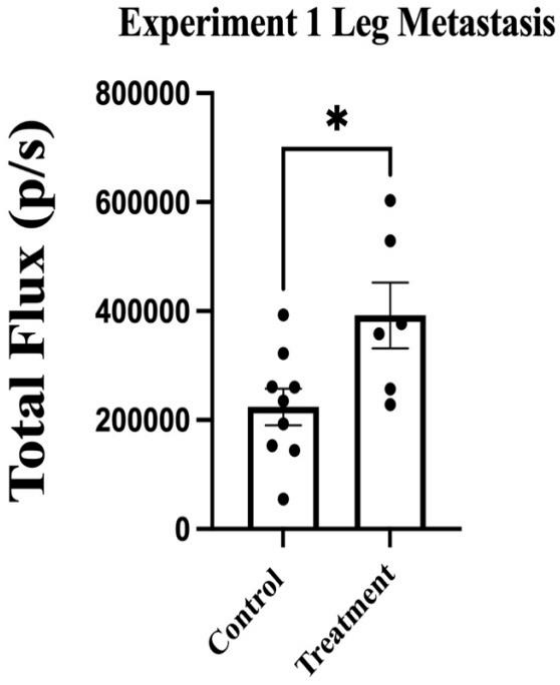

Figure 3.6 *Luminescence intensity of bone metastases in BALB/c* mice *treated with or without synthetic nanobody against subunit c (first trial).* Mice treated with either 32 ug of a synthetic nanobody against subunit c twice weekly or an equivalent volume of PBS. Mice were injected with luciferin as described in Chapter 2.5. At study endpoint, or after reaching humane endpoint criteria, then, mice were sacrificed, and hind limbs were imaged ex vivo. (N= 7 for treatment, N=9 for control) (* $p < 0.05$, error bars represent SEM).

3.5 A higher dose of the nanobody against subunit c further reduced 4T1-12B metastasis to the lungs in vivo

After observing reduced metastasis to lungs in the initial trial, we increased the dose to 64 ug of nanobody injected 3 times per week to see if a further decrease in metastasis to lungs could be achieved. The mice were divided into 2 groups, 10 mice for each. Since two mice from treatment group died at day 26 in the first experiment, we decided to shorten the study endpoint to 21 days to ensure data collection of organ metastasis for as many mice as possible. Again, no difference in tumor volume was observed at the study endpoint at day 21 (Figure 3.7).

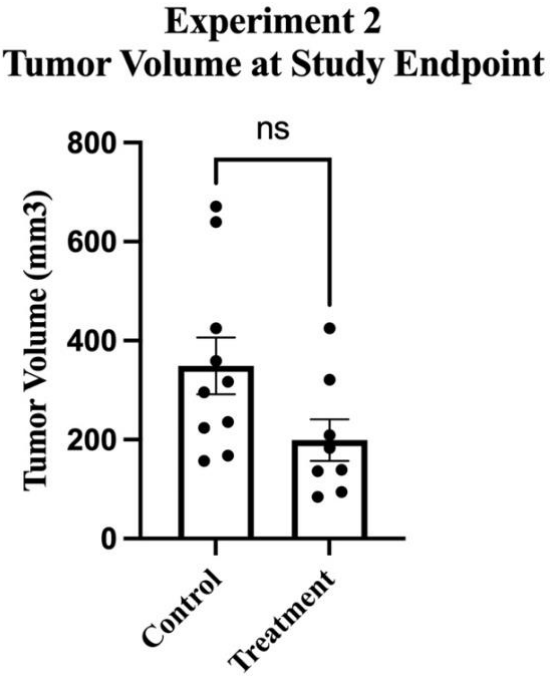

Figure 3.7 *Primary tumor volumes of BALB/c mice treated with or without synthetic nanobody against subunit c (second trial).* Mice treated with either 64 ug of a synthetic nanobody against subunit c three times per week or an equivalent volume of PBS. Tumor volumes for all mice were recorded at the time of takedown, (N= 8 for treatment, N=10 for control) (P value = 0.06, error bars represent the SEM).

Groups	Lung	Heart	Kidneys	Spleen	Liver	Brain	(Limps)
Control	(8)/10	0/10	0/10	0/10	0/10	0/10	10/10
Treatment	(2)/7	0/7	0/7	0/7	1/7	0/7	7/7

Table 3.4 *Comparison of frequency of metastases to various organs in BALB/c mice treated with or without synthetic nanobody against subunit c (second trial).* Mice treated with either 64 ug of a synthetic nanobody against subunit c three times per week or an equivalent volume of PBS. Table shows the frequency of metastasis seen in organs imaged ex vivo using IVIS bioluminescence.

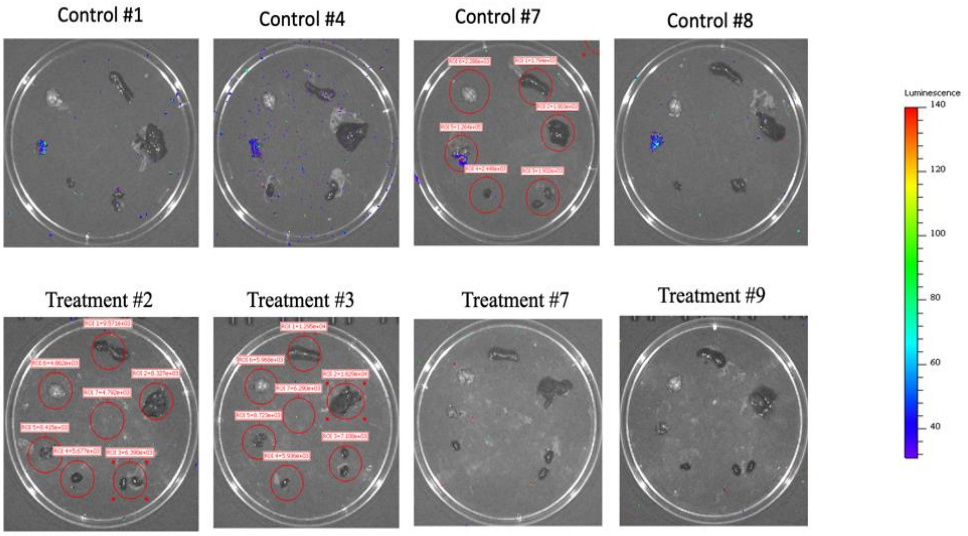

Figure 3.8 *Representative ex vivo organ IVIS images.* Top: Sample images of organs from control group treated with PBS. Organs pictures clockwise from the top are spleen, liver, kidneys, heart, lungs, and brain. Bottom: Sample images of organs from treatment group treated with 192 ug weekly of a synthetic nanobody against subunit c.

In this experiment, mouse number 1 and 5 from the treatment group died at day 15 and 21. Mouse number 4 developed a necrotic limb and was sacrificed at day 15. At the study endpoint, mice were injected with luciferin and euthanized for ex vivo tissue imaging. As shown in Table 3.4 and Figure 3.8, there was a significant reduction in metastasis to the lungs in the treatment group (2 out of 7) compared to the control group

(8 out of 10) at day 21. Mouse number 4 also showed lung metastasis when imaged at day 16. In this experiment, no significant difference in bone luminescence intensity was observed at study endpoint (day 21) as shown in Figure 3.9.

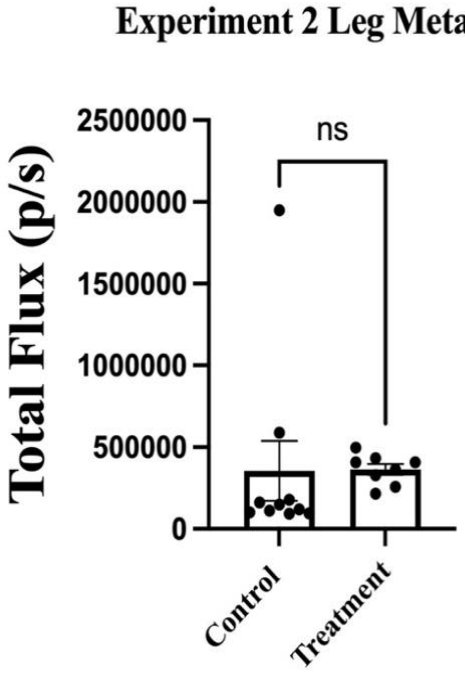

Figure 3.9 *Luminescence intensity of bone metastases in BALB/c mice treated with or without synthetic nanobody against subunit c (second trial).* Mice treated with either 64 ug of a synthetic nanobody against subunit c three times per week or an equivalent volume of PBS. Mice were injected with luciferin as described in Chapter 2.5. At study endpoint, or after reaching humane endpoint criteria, then, mice were sacrificed, and hind limbs were imaged ex vivo.) (N= 8 for treatment, N=10 for control) (* $p < 0.05$, error bars represent SEM).

To confirm these results, a third trial was conducted using an earlier passage of the same cell line. Experiments 1 and 2 employed cells at passage #10 while for the third trial, we used passage #4. Earlier passage cells did not show any difference in migration

and invasion in vitro (data not shown). Tumor volume was measured using external caliper 3 time per week.

At the study endpoint, and similar to the results of experiment 2, there was no significant difference in tumor growth between the groups at day 21 (Figure 3.10).

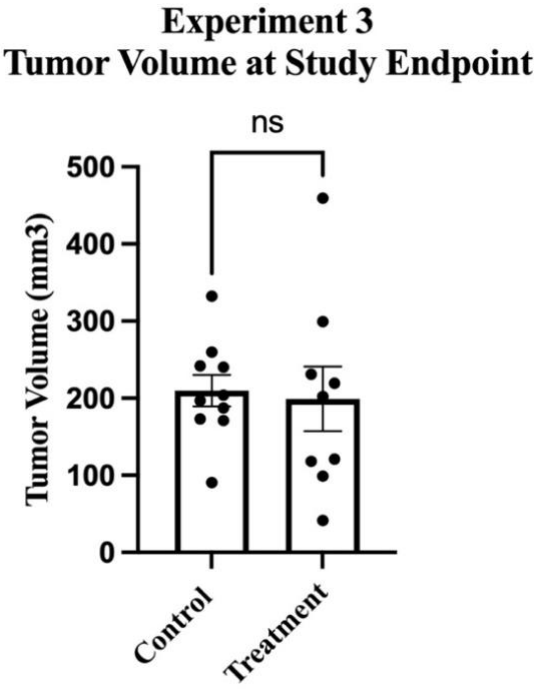

Figure 3.10 *Primary tumor volumes of BALB/c mice treated with or without synthetic nanobody against subunit c (third trial).* Mice treated with either 64 ug of a synthetic nanobody against subunit c three times per week or an equivalent volume of PBS. Tumor volumes for all mice were recorded at the time of takedown. (N= 9 for Treatment, N=10 for Control), (P value = 0.81, error bars represent the SEM).

At the study endpoint, mice were euthanized, and organs were collected for ex vivo imaging. There was significantly less metastasis overall in this trial compared to experiment 2, since only 2 mice in the control group had metastasis to the lungs, one had metastasis to liver and one to the brain. By contrast the treatment group had no metastasis to any of the organs. (Table 3.5).

Groups	Lung	Heart	Kidneys	Spleen	Liver	Brain	(Limps)
Control	(2)/10	0/10	0/10	0/10	1/10	1/10	10/10
Treatment	0/8	0/8	0/8	0/8	0/8	0/8	8/8

Table 3.5 *Comparison of frequency of metastases to various organs in BALB/c mice treated with or without synthetic nanobody against subunit c (third trial).* Mice treated with either 64 ug of a synthetic nanobody against subunit c three times per week or an equivalent volume of PBS. Table shows the frequency of metastasis seen in organs imaged ex vivo using IVIS bioluminescence.

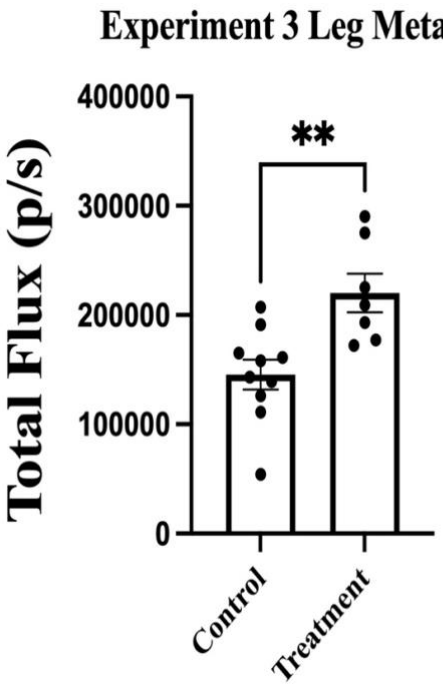

Figure 3.11 *Luminescence intensity of bone metastases in BALB/c mice treated with or without synthetic nanobody against subunit c (third trial*). Mice treated with either 64 ug of a synthetic nanobody against subunit c three times per week or an equivalent volume of PBS. Mice were injected with luciferin as described in Chapter 2.5. At study endpoint, or after reaching humane endpoint criteria, then, mice were sacrificed, and hind limbs were imaged ex vivo. (N= 7 for treatment, N=10 for control) (** $p < 0.005$, error bars represent SEM).

Mouse number 1 was euthanized due to poor body condition, and mouse 2 and 10 died on day 20, resulting in only 7 out of 10 mice surviving until the study end point for the treatment group. Similar to the first trial, the treatment group surprisingly showed a significant increase in bioluminescence signal from bone metastases (P value: <0.005) compared to the control group (Figure 3.11).

3.6 Author contributions

Chapters 3.1, 3.2, and Figure 3.3: cell culture was done by Kevin Su. In vivo bioluminescent imaging was performed by Kevin Su and Michael Collins with guidance from Min Fang from the Sahagian Lab. Figures 3.4 through 3.11: cell culture, tumor measurements and in vivo bioluminescent imaging were performed by Mohammed Alshagawi with help from Zhen Li from the Forgac lab. Michael Forgac supervised the project and revised the thesis and James Baleja revised the thesis.

Chapter 4: Discussion

4.1 Role of a subunit isoforms in breast cancer growth and metastasis

The main goal of chapters (3.1) and (3.2) was to test our hypothesis that the V-ATPase a subunit isoforms play a role in breast cancer growth and metastasis *in vivo*. We implemented the 4T1-12B breast cancer model because it is known for the ability to metastasize in immunocompetent mice (42). It is important to note that this is the first in vivo study that uses breast cancer cell lines in which V-ATPase a subunit isoforms have been selectively disrupted by use of CRISPR-mediated gene editing. It was first important to confirm that our CRISPR clones were expressing functional luciferase. Our lab has shown that none of the clones significantly differ in luciferase expression in vitro by two independent trials (Data not shown). CRISPR-mediated disruption of a4 has been shown to inhibit in vitro invasion and migration and and to decrease localization of the V-ATPase to the leading edge of 4T1-12B cells (43). Additionally, none of our clones showed significant differences in viability or proliferation *in vitro*. It was thus surprising to observe a substantial decrease in tumor growth in the a4 -/- mice.

While selectively disrupting the a4 isoform dramatically reduced tumor growth when measured by an external caliper, knocking out a2 significantly increased tumor volume (Figure 3.1 A). The a2 isoform is found mainly in intracellular compartments, such as endosomes, secretory vesicles, and Golgi (44, 46) We previously observed that gene knockdown of specific isoforms could lead to a change in expression of other isoforms as a compensatory mechanism; for instance, knockdown of a4 led to an increase in expression of a3 in MCF10CA1a cells (47). Nevertheless, knockout of a2 did not affect expression of the other isoforms in 4T1-12B cells (43). Disruption of a2 has been reported in several studies to activate different signaling pathways in breast cancer cells. The V-ATPase is

known to activate Notch signaling (48, 49) and knockdown of a2 using small interference RNA has been shown to increase Notch signaling in MDA-MB-231 cells (50). Additionally, the V-ATPase has been shown to promote Wnt signaling (51), and knockdown of a2 increased Wnt target genes in several breast cancer cell lines. Furthermore, V-ATPase inhibition might activate Wnt signaling by interfering with autophagic degradation of Dishevelled (the Wnt target protein) (52).

This study aimed to assess the role of a isoforms in breast cancer metastasis using a luciferase-expressing model that allows us to monitor the metastasis of cancer cells to different organs. In the first experiment, no detectable metastasis was observed in any of the organs because the primary tumor's strong luminescence signal prevented detection of the lower signals from metastases in live animals. In the second experiment, organs were imaged separately from the primary tumor following sacrifice and dissection (ex vivo). 15 of 15 mice had lung metastases in the control group, whereas 1 of 19 mice displayed metastases in the a4-/- group, including data from both clones (a4.5 and a4.9). Additionally, the a1 -/- group showed less metastasis than the control group (3 of 8). Although there was no difference in the number of mice showing bone metastases in the a4 -/- and control groups (Table 3.2), there was a significant reduction in the intensity of measured luminescence of bones in the a4 -/- mice (Figure 3.2). Since the a4 -/- group showed a significant reduction in primary tumor growth rate, this might explain the reduced bone metastasis. Further experiments will be required to confirm the relationship between tumor volume and the rate of metastases.

Concerning the reduction in the number of mice developing lung metastases in the a1 group and the reduced size of bone metastases in both the a1 and a3 groups, it was previously reported that a1 knockout 4T1-12B cells showed a partial reduction in a4 expression (43). This might explain the reduction of mice with lung metastasis and the decreased size of bone metastasis. Additionally, a3 disruption was only partial in 4T1-12B cells (43), suggesting a possible role of the a3 isoform in the growth of metastases in bone.

4.2 Effect of a synthetic nanobody against subunit c on breast cancer metastasis in vivo

Chapters (3.3, 3.4, and 3.5) aimed to test our hypothesis that targeting subunit c in the V0 domain using a bivalent nanobody can reduce tumor growth and metastases in vivo. Our lab has previously reported that targeting a V5 epitope tag fused to an extracellular domain of subunit c in MDA-MB-231 breast cancer cells by a monoclonal antibody can reduce in vitro invasion and migration and V-ATPase-dependent plasma membrane proton flux (40). Our lab has developed (with Proteogenix) a bivalent antibody engineered with two VHH nanobodies connected by a human CH1 and hinge region to be tested in vitro and in vivo using 4T1-12B breast cancer cells. We raised the nanobody against the N-terminal tail of subunit c since it has the highest degree of extension from the plasma membrane compared to other epitopes, based on the structure of rat and bovine V-ATPases (53, 54).

Because the c subunit sequence is relatively conserved among mammals, it might be challenging to produce an antibody through animal immunization (55). Thus, an in vitro phage display approach was taken. One of the main advantages of choosing bivalent nanobodies versus conventional antibodies is the lower molecular weight of VHH

nanobodies (~15 kDa) compared to IgG (~150 kDa) (56), which might overcome the problem of tissue penetration associated with monoclonal antibodies (57, 56). Invasion and migration assays were performed using 4T1-12B cells as described in Chapter (2.2). Significantly, our nanobody caused a ~53% reduction in cell migration and an ~83% reduction in cell invasion by 4T1-12B cells (Figure 3.3A, 3.3B).

The first trial *in vivo* tested the effect of our nanobody on tumor growth and metastasis of 4T1-12B cells orthotopically implanted in BALB/c mice. Both the control and treatment groups were split into two subgroups. Half of the mice in each group were implanted with 1.5×10^6 cells, while half were implanted with 1×10^6 cells. It's important to note that the control group mistakenly received 10X PBS instead of 1XPBS in place of the nanobody administration, but this was not expected to affect tumor growth or metastasis. Interestingly, a significant reduction in lung metastases was observed in the group treated with the nanobody (100 ul of 0.32 mg/ml twice per week) compared to the control group (Table 3.3). Nevertheless, there was no significant difference in tumor volume. This may suggest that the nanobody may have bound to and neutralized circulating tumor cells, thus preventing metastasis to the lungs, yet without altering growth of the primary tumor. The fact that the nanobody did not prevent metastasis to bone may be explained by the fact that breast tumor cells employ osteoclasts to invade bone, and the nanobody may have had no effect on this ability of the tumor cells. Injecting a higher dose (200 ul containing 0.32 mg/ml three times per week) in the second trial further decreased the number of mice with lung metastasis (Table 3.4), without any effect on tumor growth or reduction in bone metastasis. No difference in the intensity of the luciferase signal in the bone was observed between the groups. In the third trial, we

used a somewhat earlier passage of 4T1-12B cells and were surprised to see fewer mice with lung metastasis in the control group (2/10).

Nevertheless, no mice in the treatment group showed lung metastases, consistent with our earlier findings. Based on our results this far, we plan several modifications to our protocol. First, we plan to implant a smaller number of cells (1×10^5 cells instead of 1×10^6 cells) to allow the study duration to be extended before the development of necrosis, thus increasing the likelihood of metastasis. Second, we plan to use a lower dose of nanobody in our subsequent experiments, since several mice in the treatment group died before the study endpoint, possibly due to an adverse immune reaction to the nanobody, which has an alpaca origin. Finally, we plan to test our nanobody using a different route of administration, namely intravenously, since this may allow the nanobody to more directly access tumor cells which have escaped the primary tumor into the circulation.

Our preliminary results thus demonstrate that targeting plasma membrane V-ATPases in 4T1-12B breast cancer cells using our selective nanobody against subunit c reduces lung metastasis in vivo and support the hypothesis that plasma membrane V-ATPases represent an important and novel target for limiting breast cancer metastasis.

Chapter 5: Bibliography

1. Forgac, M. (2007) Vacuolar ATPases: rotary proton pumps in physiology and pathophysiology. *Nat. Rev. Mol. Cell Biol.* **8**, 917–929
2. Nishi, T., and Forgac, M. (2002) The vacuolar (H+)-ATPases — nature′s most versatile proton pumps. *Nat. Rev. Mol. Cell Biol.* **3**, 94–103
3. Cross, R. L., and Müller, V. (2004) The evolution of A-, F-, and V-type ATP synthases and ATPases: reversals in function and changes in the H^+/ATP coupling ratio. *FEBS Lett.* **576**, 1–4
4. Cotter, K., Stransky, L., McGuire, C., and Forgac, M. (2015) Recent Insights into the Structure, Regulation, and Function of the V-ATPases. *Trends Biochem. Sci.* **40**, 611–622
5. Maxfield, F. R., and McGraw, T. E. (2004) Endocytic recycling. *Nat. Rev. Mol. Cell Biol.* **5**, 121–132
6. Grove, J., and Marsh, M. (2011) The cell biology of receptor-mediated virus entry. *J. Cell Biol.* **195**, 1071–1082
7. Gruenberg, J., and van der Goot, F. G. (2006) Mechanisms of pathogen entry through the endosomal compartments. *Nat. Rev. Mol. Cell Biol.* **7**, 495–504
8. Farsi, Z., Preobraschenski, J., van den Bogaart, G., Riedel, D., Jahn, R., and Woehler, A. (2016) Single-vesicle imaging reveals different transport mechanisms between glutamatergic and GABAergic vesicles. *Science*. **351**, 981–984
9. Das, G., Shravage, B. V., and Baehrecke, E. H. (2012) Regulation and Function of Autophagy during Cell Survival and Cell Death. *Cold Spring Harb. Perspect. Biol.* **4**, a008813–a008813
10. Nakatogawa, H., Suzuki, K., Kamada, Y., and Ohsumi, Y. (2009) Dynamics and diversity in autophagy mechanisms: lessons from yeast. *Nat. Rev. Mol. Cell Biol.* **10**, 458–467
11. Feng, Y., He, D., Yao, Z., and Klionsky, D. J. (2014) The machinery of macroautophagy. *Cell Res.* **24**, 24–41
12. Kawai, A., Uchiyama, H., Takano, S., Nakamura, N., and Ohkuma, S. (2007) Autophagosome-Lysosome Fusion Depends on the pH in Acidic Compartments in CHO Cells. *Autophagy*. **3**, 154–157
13. Yamamoto, A., Tagawa, Y., Yoshimori, T., and Moriyama, Y. Bafilomycin Ai Prevents Maturation of Autophagic Vacuoles by Inhibiting Fusion bH-e4t-IwI-Eeen ACeullstophagosomesand Lysosomesin Rat HepatomaCell Line,
14. Galluzzi, L., Bravo-San Pedro, J. M., Levine, B., Green, D. R., and Kroemer, G. (2017) Pharmacological modulation of autophagy: therapeutic potential and persisting obstacles. *Nat. Rev. Drug Discov.* **16**, 487–511
15. Miranda, K. C., Karet, F. E., and Brown, D. (2010) An Extended Nomenclature for Mammalian V-ATPase Subunit Genes and Splice Variants. *PLoS ONE*. **5**, e9531
16. Bodzęta, A., Kahms, M., and Klingauf, J. (2017) The Presynaptic v-ATPase Reversibly Disassembles and Thereby Modulates Exocytosis but Is Not Part of the Fusion Machinery. *Cell Rep.* **20**, 1348–1359
17. Hurtado-Lorenzo, A., Skinner, M., Annan, J. E., Futai, M., Sun-Wada, G.-H., Bourgoin, S., Casanova, J., Wildeman, A., Bechoua, S., Ausiello, D. A., Brown, D.,

and Marshansky, V. (2006) V-ATPase interacts with ARNO and Arf6 in early endosomes and regulates the protein degradative pathway. *Nat. Cell Biol.* **8**, 124–136

18. Toyomura, T., Murata, Y., Yamamoto, A., Oka, T., Sun-Wada, G.-H., Wada, Y., and Futai, M. (2003) From Lysosomes to the Plasma Membrane. *J. Biol. Chem.* **278**, 22023–22030
19. Oka, T., Murata, Y., Namba, M., Yoshimizu, T., Toyomura, T., Yamamoto, A., Sun-Wada, G.-H., Hamasaki, N., Wada, Y., and Futai, M. (2001) a4, a Unique Kidney-specific Isoform of Mouse Vacuolar H+-ATPase Subunit a. *J. Biol. Chem.* **276**, 40050–40054
20. Smith, A. N., Borthwick, K. J., and Karet, F. E. (2002) Molecular cloning and characterization of novel tissue-specific isoforms of the human vacuolar H1-ATPase C, G and d subunits, and their evaluation in autosomal recessive distal renal tubular acidosisq
21. Sun-Wada, G.-H., Imai-Senga, Y., Yamamoto, A., Murata, Y., Hirata, T., Wada, Y., and Futai, M. (2002) A Proton Pump ATPase with Testis-specific E1-Subunit Isoform Required for Acrosome Acidification. *J. Biol. Chem.* **277**, 18098–18105
22. Shum, W. W. C., Da Silva, N., Brown, D., and Breton, S. (2009) Regulation of luminal acidification in the male reproductive tract *via* cell–cell crosstalk. *J. Exp. Biol.* **212**, 1753–1761
23. Stransky, L., Cotter, K., and Forgac, M. (2016) The Function of V-ATPases in Cancer. *Physiol. Rev.* **96**, 1071–1091
24. Collins, M. P., and Forgac, M. (2018) Regulation of V-ATPase Assembly in Nutrient Sensing and Function of V-ATPases in Breast Cancer Metastasis. *Front. Physiol.* **9**, 902
25. Webb, B. A., Chimenti, M., Jacobson, M. P., and Barber, D. L. (2011) Dysregulated pH: a perfect storm for cancer progression. *Nat. Rev. Cancer*. **11**, 671–677
26. von Schwarzenberg, K., Wiedmann, R. M., Oak, P., Schulz, S., Zischka, H., Wanner, G., Efferth, T., Trauner, D., and Vollmar, A. M. (2013) Mode of Cell Death Induction by Pharmacological Vacuolar H+-ATPase (V-ATPase) Inhibition. *J. Biol. Chem.* **288**, 1385–1396
27. Schempp, C. M., von Schwarzenberg, K., Schreiner, L., Kubisch, R., Müller, R., Wagner, E., and Vollmar, A. M. (2014) V-ATPase Inhibition Regulates Anoikis Resistance and Metastasis of Cancer Cells. *Mol. Cancer Ther.* **13**, 926–937
28. Cotter, K., Liberman, R., Sun-Wada, G., Wada, Y., Sgroi, D., Naber, S., Brown, D., Breton, S., and Forgac, M. (2016) The a3 isoform of subunit a of the vacuolar ATPase localizes to the plasma membrane of invasive breast tumor cells and is overexpressed in human breast cancer. *Oncotarget*. **7**, 46142–46157
29. Lu, Q., Lu, S., Huang, L., Wang, T., Wan, Y., Zhou, C. X., Zhang, C., Zhang, Z., and Li, X. (2013) The expression of V-ATPase is associated with drug resistance and pathology of non-small-cell lung cancer. *Diagn. Pathol.* **8**, 145
30. Capecci, J., and Forgac, M. (2013) The Function of Vacuolar ATPase (V-ATPase) a Subunit Isoforms in Invasiveness of MCF10a and MCF10CA1a Human Breast Cancer Cells. *J. Biol. Chem.* **288**, 32731–32741
31. Hinton, A., Sennoune, S. R., Bond, S., Fang, M., Reuveni, M., Sahagian, G. G., Jay, D., Martinez-Zaguilan, R., and Forgac, M. (2009) Function of a Subunit Isoforms of

the V-ATPase in pH Homeostasis and in Vitro Invasion of MDA-MB231 Human Breast Cancer Cells. *J. Biol. Chem.* **284**, 16400–16408
32. Sennoune, S. R., Bakunts, K., Martınez, G. M., Chua-Tuan, J. L., Kebir, Y., Attaya, M. N., and Martınez-Zaguilan, R. (2004) Vacuolar Hƨ-ATPase in human breast cancer cells with distinct metastatic potential: distribution and functional activity. **286**, 10
33. McGuire, C. M., Collins, M. P., Sun-Wada, G., Wada, Y., and Forgac, M. (2019) Isoform-specific gene disruptions reveal a role for the V-ATPase subunit a4 isoform in the invasiveness of 4T1-12B breast cancer cells. *J. Biol. Chem.* **294**, 11248–11258
34. Wojtkowiak, J. W., Verduzco, D., Schramm, K. J., and Gillies, R. J. (2011) Drug Resistance and Cellular Adaptation to Tumor Acidic pH Microenvironment. *Mol. Pharm.* **8**, 2032–2038
35. Vukovic, V., and Tannock, I. (1997) Influence of low pH on cytotoxicity of paclitaxel, mitoxantrone and topotecan. *Br. J. Cancer*. **75**, 1167–1172
36. Ouar, Z., Bens, M., Vignes, C., Paulais, M., Pringel, C., Fleury, J., Lacave, R., and Vandewalle, A. (2003) Inhibitors of vacuolar HT-ATPase impair the preferential accumulation of daunomycin in lysosomes and reverse the resistance to anthracyclines in drug-resistant renal epithelial cells
37. Luciani, F., Spada, M., De Milito, A., Molinari, A., Rivoltini, L., Montinaro, A., Marra, M., Lugini, L., Logozzi, M., Lozupone, F., Federici, C., Iessi, E., Parmiani, G., Arancia, G., Belardelli, F., and Fais, S. (2004) Effect of Proton Pump Inhibitor Pretreatment on Resistance of Solid Tumors to Cytotoxic Drugs. *JNCI J. Natl. Cancer Inst.* **96**, 1702–1713
38. Lambert, A. W., Pattabiraman, D. R., and Weinberg, R. A. (2017) Emerging Biological Principles of Metastasis. *Cell*. **168**, 670–691
39. Chung, C., Mader, C. C., Schmitz, J. C., Atladottir, J., Fitchev, P., Cornwell, M. L., Koleske, A. J., Crawford, S. E., and Gorelick, F. (2011) The vacuolar-ATPase modulates matrix metalloproteinase isoforms in human pancreatic cancer. *Lab. Invest.* **91**, 732–743
40. Cotter, K., Capecci, J., Sennoune, S., Huss, M., Maier, M., Martinez-Zaguilan, R., and Forgac, M. (2015) Activity of Plasma Membrane V-ATPases Is Critical for the Invasion of MDA-MB231 Breast Cancer Cells. *J. Biol. Chem.* **290**, 3680–3692
41. Tomayko, M. M., and Reynolds, C. P. (1989) Determination of subcutaneous tumor size in athymic (nude) mice. *Cancer Chemother. Pharmacol.* **24**, 148–154
42. Tao, K., Fang, M., Alroy, J., and Sahagian, G. G. (2008) Imagable 4T1 model for the study of late stage breast cancer. *BMC Cancer*. **8**, 228
43. McGuire, C. M., Collins, M. P., Sun-Wada, G., Wada, Y., and Forgac, M. (2019) Isoform-specific gene disruptions reveal a role for the V-ATPase subunit a4 isoform in the invasiveness of 4T1-12B breast cancer cells. *J. Biol. Chem.* **294**, 11248–11258
44. Toyomura, T., Murata, Y., Yamamoto, A., Oka, T., Sun-Wada, G.-H., Wada, Y., and Futai, M. (2003) From lysosomes to the plasma membrane: localization of vacuolar-type H+ -ATPase with the a3 isoform during osteoclast differentiation. *J. Biol. Chem.* **278**, 22023–22030

45. Pietrement, C., Sun-Wada, G.-H., Silva, N. D., McKee, M., Marshansky, V., Brown, D., Futai, M., and Breton, S. (2006) Distinct expression patterns of different subunit isoforms of the V-ATPase in the rat epididymis. *Biol. Reprod.* **74**, 185–194
46. Hurtado-Lorenzo, A., Skinner, M., El Annan, J., Futai, M., Sun-Wada, G.-H., Bourgoin, S., Casanova, J., Wildeman, A., Bechoua, S., Ausiello, D. A., Brown, D., and Marshansky, V. (2006) V-ATPase interacts with ARNO and Arf6 in early endosomes and regulates the protein degradative pathway. *Nat. Cell Biol.* **8**, 124–136
47. Capecci, J., and Forgac, M. (2013) The function of vacuolar ATPase (V-ATPase) a subunit isoforms in invasiveness of MCF10a and MCF10CA1a human breast cancer cells. *J. Biol. Chem.* **288**, 32731–32741
48. Yan, Y., Denef, N., and Schüpbach, T. (2009) The Vacuolar Proton Pump, V-ATPase, Is Required for Notch Signaling and Endosomal Trafficking in Drosophila. *Dev. Cell*. **17**, 387–402
49. Sethi, N., Yan, Y., Quek, D., Schupbach, T., and Kang, Y. (2010) Rabconnectin-3 Is a Functional Regulator of Mammalian Notch Signaling. *J. Biol. Chem.* **285**, 34757–34764
50. Pamarthy, S., Jaiswal, M. K., Kulshreshtha, A., Katara, G. K., Gilman-Sachs, A., and Beaman, K. D. (2015) The Vacuolar ATPase a2-subunit regulates Notch signaling in triple-negative breast cancer cells. *Oncotarget*. **6**, 34206–34220
51. Cruciat, C.-M., Ohkawara, B., Acebron, S. P., Karaulanov, E., Reinhard, C., Ingelfinger, D., Boutros, M., and Niehrs, C. (2010) Requirement of Prorenin Receptor and Vacuolar H^+-ATPase–Mediated Acidification for Wnt Signaling. *Science*. **327**, 459–463
52. Gao, C., Cao, W., Bao, L., Zuo, W., Xie, G., Cai, T., Fu, W., Zhang, J., Wu, W., Zhang, X., and Chen, Y.-G. (2010) Autophagy negatively regulates Wnt signalling by promoting Dishevelled degradation. *Nat. Cell Biol.* **12**, 781–790
53. Abbas, Y. (2020) Structure of V-ATPase from mammalian brain. *Acta Crystallogr. Sect. Found. Adv.* **76**, a123–a123
54. Wang, R., Long, T., Hassan, A., Wang, J., Sun, Y., Xie, X.-S., and Li, X. (2020) Cryo-EM structures of intact V-ATPase from bovine brain. *Nat. Commun.* **11**, 3921
55. Nemazee, D. (2017) Mechanisms of central tolerance for B cells. *Nat. Rev. Immunol.* **17**, 281–294
56. Steeland, S., Vandenbroucke, R. E., and Libert, C. (2016) Nanobodies as therapeutics: big opportunities for small antibodies. *Drug Discov. Today*. **21**, 1076–1113
57. Minchinton, A. I., and Tannock, I. F. (2006) Drug penetration in solid tumours. *Nat. Rev. Cancer*. **6**, 583–592